We are IntechOpen, the world's leading publisher of Open Access books Built by scientists, for scientists

6,900
Open access books available

185,000
International authors and editors

200M
Downloads

Our authors are among the

154
Countries delivered to

TOP 1%
most cited scientists

12.2%
Contributors from top 500 universities



WEB OF SCIENCE™

Selection of our books indexed in the Book Citation Index in Web of Science™ Core Collection (BKCI)

Interested in publishing with us?
Contact book.department@intechopen.com

Numbers displayed above are based on latest data collected.
For more information visit www.intechopen.com



Chapter

Thermal Radiation and Thermal Diffusion for Soret and Dufour's Effects on MHD Flow over Rotating Infinite Disk

Gamal M. Abdel-Rahman and Faiza M.N. El-fayez

Abstract

In general, the thermal radiation and thermal diffusion effects over an electrically conducting, Newtonian fluid in a steady laminar magnetohydrodynamic convective flow over a porous rotating infinite disk with the consideration of heat and mass transfer in the presence of Soret and Dufour's diffusion effects have been obtained and studied numerically. The governing continuity, momentum, energy and concentration equations are converted into a system of non-linear ordinary differential equations by means of similarity transformation. The resulting system of coupled non-linear ordinary differential equations is solved numerically. In this chapter, numerical results were presented for velocity (radial, axial and tangential), temperature, concentration and pressure profiles for different parameters of the problem Also, the effects of the pertinent parameters on the radial and tangential skin friction, the rate of heat and mass transfer are obtained and discussed numerically and illustrated graphically.

Keywords: MHD, heat and mass transfer, thermal radiation, slip flow, porous medium, rotating disk

1. Introduction

The flow due to rotating disks is of great interest in many practical and engineering aspects. Rotating disk flows of electrically conducting fluids have practical applications in many areas, such as rotating machinery, lubrication, oceanography, computer storage devices, viscometer and crystal growth processes etc. Also, the study is interesting from the mathematical point of view. During the last two decades, research on renewable energy sources, as for example, solar, wind energy or energy from hydro-power and the preparation of oxygenated additives to blend diesel fuel, has been intensified.

Pioneering study of fluid flow due to an infinite rotating disk was carried by authors [1–3]. Chemical reactions usually accompany a large amount of exothermic and endothermic reactions. These characteristics can be easily seen in a lot of industrial processes, it has been realized that it is not always permissible to neglect the convection effects in porous constructed chemical reactors [4]. The reaction produced in a porous medium was extraordinarily in common, such as the topic of

IntechOpen

PEM fuel cells modules and the polluted underground water because of discharging the toxic substance, etc.

Fourier's law, for instance, described the relation between energy flux and temperature gradient. In other aspects, Fick's law was determined by the correlation of mass flux and concentration gradient. Moreover, it was found that energy flux can also be generated by composition gradients, pressure gradients, or body forces. The energy flux caused by a composition gradient was discovered in 1873 by Dufour and was correspondingly referred to the Dufour effect.

It was also called the diffusion-thermo effect. On the other hand, mass flux can also be created by a temperature gradient, as was established by Soret. This is the thermal-diffusion effect. In general, the thermal-diffusion and the diffusion-thermo effects were of a smaller order of magnitude than the effects described by Fourier's or Fick's law and were often neglected in heat and mass transfer processes. There were still some exceptional conditions. The thermal-diffusion effect has been utilized for isotope separation and in mixtures between gases with very light molecular weight (H_2, He) and of medium molecular weight (N_2, air), the diffusion-thermo effect was found to be of a magnitude such that it may not be neglected in certain conditions [5].

The first traceable interest in magnetohydrodynamics (MHD) flow was in 1907, when Northrop built an MHD pump prototype [6, 7]. Since then, analysis of the effects of both rotation and magnetic fields on fluid flows has been an active area of research. While technology expanded in many directions, the subject of MHD has developed in the use of magnetic fields and the range of fluid and thermal processes by [8–13]. This study considers the effect of slip as a result of rarefied effect, a type of flow commonly encountered in many engineering tasks such as high altitude flight, micro-machines, vacuum technology, aerosol reactors, etc. In this study, the slip and no-slip regimes that lie in the range $0.1 > K_n > 0$ are considered.
A completely different extension of von Karman's one-disk problem is the analysis of Sparrow et al. [14]. They considered the flow of a Newtonian fluid due to the rotation of a porous-surfaced disk and for that purpose replaced the conventional no-slip boundary conditions at the disk surface with a set of linear slip flow conditions. A substantial reduction in torque then occurred as a result of surface slip. Recently Frusteri and Osalusi [15] studied the effects of variable properties on MHD and slip flow over a porous rotating disk.

In all these studies Soret and Dufour effects were assumed to be negligible. Such effects are significant when density differences exist in the flow regime. For example, when species are introduced at a surface in fluid domain, with different (lower) density than the surrounding fluid, both Soret (thermo-diffusion) and Dufour (diffusion-thermal) effects can be influential. An analytical study of convection along a horizontal cylinder for a Helium-air system was reported subsequently by Sparrow et al. [16]. In view of the importance of above mentioned effects, Maleque [17] studied Soret effect on convective heat and mass transfer past a rotating porous disk and he neglected the Dufour effect. Ahmed [18] investigated the Dufour and Soret effects on free convective heat and mass transfer over a stretching surface considering suction or injection. Recently, numerical study of free convection magnetohydrodynamic heat and mass transfer due to a stretching surface under saturated porous medium with Soret and Dufour effects was also discussed by Anwar Beg et al. [19].

In these two papers [15, 20] they have studied the effect of the magnetic field on the equations of motion that I found them used in the cylindrical coordinate, although the magnetic field parameters are in the Cartesian coordinate, which is wrong.

2. Mathematical formulation

Consider the steady, axially symmetric, incompressible flow of an electrically conducting fluid with heat and mass transfer flow due to a rotating porous disk in the presence of radiation has been considered. Assume that the fluid is infinite in extent in the positive z-direction. Let (r, φ, z) be the set of cylindrical polar coordinates and let the disk rotate with constant angular velocity Ω and is placed at $z = 0$. The components of the flow velocity are (u, v, w) in the directions of increasing (r, φ, z), respectively. p, T and C are the pressure, the temperature and the concentration distribution, respectively. The surface of the rotating disk is maintained at a uniform temperature T_w and uniform concentration C_w. Far away from the surface, the free stream is kept at a constant temperature T_∞, at a constant concentration C_∞ and at a constant pressure p_∞. The fluid is assumed to be gray, emitting and absorbing heat, but not scattering medium and is assumed to be Newtonian. The physical model and geometrical coordinates are shown in **Figure 1**.

The MHD body forces $\bar{J} \times \overline{B}$ the Maxwell's equations:

$$div\,\overline{B} = 0,\ Curl\,\overline{B} = \mu_m \bar{J} \text{ and } div\,\overline{E} = 0$$

where $\bar{J}$ is the electric current density, $\overline{B} = B + b$ is the total magnetic field, μ_m is the magnetic permeability and b is the induced magnetic field. The external uniform magnetic field B is imposed in the direction normal to the surface of the disk which is assumed unchanged by taking small magnetic Reynolds number, so that the flow induction distortion of the applied magnetic field can be neglected as in the case with most of conducting fluids. In addition, a uniform suction is applied at the surface of the disk for the entire range.

The magnetic body force $\bar{J} \times \overline{B}$ takes the form $\sigma(\overline{V} \times \overline{B}) \times \overline{B}$, therefore, $\sigma(\overline{V} \times \overline{B}) \times \overline{B} = -\sigma B^2 \overline{V}/r$, where σ is the electrical conductivity of fluid and $\overline{V}$ is

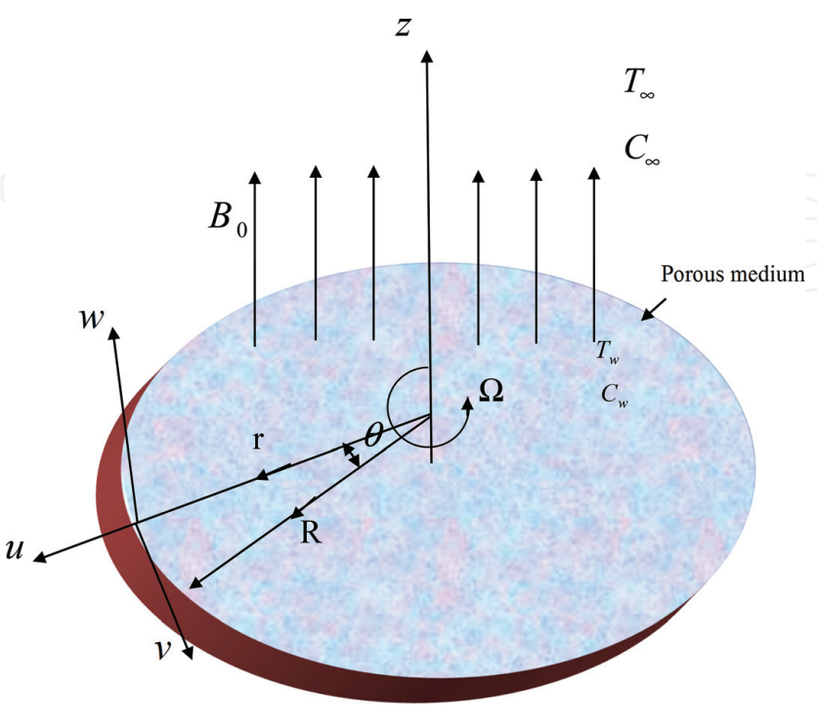


Figure 1.
Schematic diagram of the problem.

velocity vector $\overline{V} = (u, v, w)$ and $\overline{B} = (0, 0, B)$. The Lorentz force (MHD body force) has two components:

$$F_r = -\sigma B^2 u/r, F_\theta = -\sigma B^2 v/r.$$

Under these assumptions, the governing equations for the continuity, momentum, energy and concentration in laminar incompressible flow can be written as follows:

$$\frac{\partial u}{\partial r} + \frac{u}{r} + \frac{\partial w}{\partial z} = 0\ , \tag{1}$$

$$u\frac{\partial u}{\partial r} - \frac{v^2}{r} + w\frac{\partial u}{\partial z} = -\frac{1}{\rho}\frac{\partial p}{\partial r} + \nu\left(\frac{\partial^2 u}{\partial r^2} + \frac{1}{r}\frac{\partial u}{\partial r} - \frac{u}{r^2} + \frac{\partial^2 u}{\partial z^2}\right) - \frac{\sigma B^2}{\rho r}u - \frac{\nu}{K_1^*}u + g\beta_T(T - T_\infty) + g\beta_C(C - C_\infty), \tag{2}$$

$$u\frac{\partial v}{\partial r} + \frac{uv}{r} + w\frac{\partial v}{\partial z} = \nu\left(\frac{\partial^2 v}{\partial r^2} + \frac{1}{r}\frac{\partial v}{\partial r} - \frac{v}{r^2} + \frac{\partial^2 v}{\partial z^2}\right) - \frac{\sigma B^2}{\rho r}v - \frac{\nu}{K_1^*}v, \tag{3}$$

$$u\frac{\partial w}{\partial r} + w\frac{\partial w}{\partial z} = -\frac{1}{\rho}\frac{\partial p}{\partial z} + \nu\left(\frac{\partial^2 w}{\partial r^2} + \frac{1}{r}\frac{\partial w}{\partial r} + \frac{\partial^2 w}{\partial z^2}\right), \tag{4}$$

$$u\frac{\partial T}{\partial r} + w\frac{\partial T}{\partial z} = \frac{k}{\rho c_p}\left(\frac{\partial^2 T}{\partial r^2} + \frac{1}{r}\frac{\partial T}{\partial r} + \frac{\partial^2 T}{\partial z^2}\right) - \frac{1}{\rho c_p}\frac{\partial q_r}{\partial z} + \frac{D k_T}{c_s c_p}\left(\frac{\partial^2 C}{\partial r^2} + \frac{1}{r}\frac{\partial C}{\partial r} + \frac{\partial^2 C}{\partial z^2}\right) + \frac{\sigma B^2}{\rho c_p r}u^2 + \frac{Q}{\rho c_p}(T - T_\infty), \tag{5}$$

$$u\frac{\partial C}{\partial r} + w\frac{\partial C}{\partial z} = D\left(\frac{\partial^2 C}{\partial r^2} + \frac{1}{r}\frac{\partial C}{\partial r} + \frac{\partial^2 C}{\partial z^2}\right) + \frac{D k_T}{T_m}\left(\frac{\partial^2 T}{\partial r^2} + \frac{1}{r}\frac{\partial T}{\partial r} + \frac{\partial^2 T}{\partial z^2}\right) - k_1(C - C_\infty) \tag{6}$$

When the mean free path of the fluid particle is comparable to the characteristic dimensions of the flow field domain, Naiver-Stokes equations break down since the assumption of continuum media fails. In the range of $0.1 < k_n < 10$ Knudsen Number, the higher order continuum equation, for example, Burnett equation should be used. For the range of $0.001 \le k_n \le 0.1$, no slip boundary conditions cannot be used and should be replaced with the following expression (Gad-el-Hak [20]):

$$U_t = \frac{2 - \xi}{\xi}\lambda\frac{\partial U_t}{\partial n}, \tag{7}$$

Where U_t is the tangential velocity, n is the normal direction to the wall, ξ is the tangent momentum accommodation coefficient and λ is the mean free path. For $k_n < 0.001$, the no-slip boundary condition is valid, therefore, the velocity at the surface is equal to zero. In this study the slip and the no-slip regimes of the Knudsen number that lies in the range $0.1 > k_n > 0$ is considered. By using Eq. (7), the appropriate boundary conditions for the flow induced by an infinite disk $(z = 0)$ which rotates with constant angular velocity Ω subjected to uniform suction w_0 through the disk are given by

$$\begin{aligned} z = 0: &\quad u = \frac{2 - \xi}{\xi}\lambda\frac{\partial u}{\partial z},\ v = \Omega r + \frac{2 - \xi}{\xi}\lambda\frac{\partial v}{\partial z},\ w = w_0,\ T = T_w,\ C = C_w, \\ z \to \infty: &\quad u \to 0, v \to 0,\quad T \to T_\infty,\quad C \to C_\infty,\ p \to p_\infty. \end{aligned} \tag{8}$$

where k is the thermal conductivity, $\nu = \mu/\rho$ is the kinematic viscosity of the ambient fluid, σ is the electrical conductivity, K_1^* is the permeability of the porous medium, g is the gravitational acceleration, β_T and β_C are the expansion coefficients of temperature and concentration, ρ, μ and c_p are the density, dynamic viscosity and the specific heat at constant pressure, respectively, Q is the volumetric heat generation/absorption rate, D is the molecular diffusion coefficient, k_T, c_s, T_m and q_r are the thermal-diffusion rate, concentration susceptibility, the mean fluid temperature and the radiative heat flux. Using the Rosseland approximation (Rashed [21]), the radiative heat flux q_r could be expressed by

$$q_r = -\frac{4\sigma^*}{3k^*}\frac{\partial T^4}{\partial z} \tag{9}$$

Where the σ^* represents the Stefan-Boltzman constant and k^* is the Rosseland mean absorption coefficient.

Assuming that the temperature difference within the flow is sufficiently small such that T^4 could be approached as the linear function of temperature

$$T^4 \cong 4T_\infty^3 T - 3T_\infty^4 \tag{10}$$

For the flow under study, it is relevant to assume that the applied magnetic field $B(r)$ has the form cobble [22] $B = B_0\sqrt{r}$, where B_0 is constant magnetic flux density.

To obtain the non-dimensional form of the above equations, the following dimensionless variables are introduced.

$$\begin{aligned} &\overline{R} = \frac{r}{L},\ \overline{Z} = \frac{z}{L},\ \overline{U} = \frac{u}{\Omega L},\ \overline{V} = \frac{v}{\Omega L},\ \overline{\lambda} = \frac{\lambda}{L}, \overline{W} = \frac{w}{\Omega L}, \overline{P} = \frac{p - p_\infty}{\rho\Omega^2 L^2},\\ &\overline{\nu} = \frac{\nu}{\Omega L^2},\ \overline{k_1} = \frac{k_1}{L^2},\ \overline{T} = \frac{T - T_\infty}{T_w - T_\infty},\ \overline{C} = \frac{C - C_\infty}{C_w - C_\infty},\ k_1^* = \frac{\overline{k_*}}{L^2} \end{aligned} \tag{11}$$

Substituting Eqs. (9)–(11) in Eqs. (1)–(6), we obtain the following dimensionless equations:

$$\frac{\partial \overline{U}}{\partial \overline{R}} + \frac{\overline{U}}{\overline{R}} + \frac{\partial \overline{W}}{\partial \overline{Z}} = 0\ , \tag{12}$$

$$\begin{aligned} \overline{U}\frac{\partial \overline{U}}{\partial \overline{R}} - \frac{\overline{V^2}}{\overline{R}} + \overline{W}\frac{\partial \overline{U}}{\partial \overline{Z}} = &-\frac{\partial \overline{P}}{\partial \overline{R}} + \overline{\nu}\left(\frac{\partial^2 \overline{U}}{\partial \overline{R^2}} + \frac{1}{\overline{R}}\frac{\partial \overline{U}}{\partial \overline{R}} - \frac{\overline{U}}{\overline{R^2}} + \frac{\partial^2 \overline{U}}{\partial \overline{Z^2}}\right) - \frac{\sigma B_0^2}{\rho\Omega}\overline{U} - \frac{\overline{\nu}}{\overline{k_1}}\overline{U}\\ &+ \frac{g\beta_T(T_w - T_\infty)}{\Omega^2 L}\overline{T} + \frac{g\beta_c(C_w - C_\infty)}{\Omega^2 L}\overline{C}, \end{aligned} \tag{13}$$

$$\overline{U}\frac{\partial \overline{V}}{\partial \overline{R}} - \frac{\overline{U}\,\overline{V}}{\overline{R}} + \overline{W}\frac{\partial \overline{V}}{\partial \overline{Z}} = \overline{\nu}\left(\frac{\partial^2 \overline{V}}{\partial \overline{R^2}} + \frac{1}{\overline{R}}\frac{\partial \overline{V}}{\partial \overline{R}} - \frac{\overline{V}}{\overline{R^2}} + \frac{\partial^2 \overline{V}}{\partial \overline{Z^2}}\right) - \frac{\sigma B_0^2}{\rho\Omega}\overline{V} - \frac{\overline{\nu}}{\overline{k_1}}\overline{V}, \tag{14}$$

$$\overline{U}\frac{\partial \overline{W}}{\partial \overline{R}} + \overline{W}\frac{\partial \overline{W}}{\partial \overline{Z}} = -\frac{\partial \overline{P}}{\partial \overline{Z}} + \overline{\nu}\left(\frac{\partial^2 \overline{W}}{\partial \overline{R^2}} + \frac{1}{\overline{R}}\frac{\partial \overline{W}}{\partial \overline{R}} + \frac{\partial^2 \overline{W}}{\partial \overline{Z^2}}\right), \tag{15}$$

$$\begin{aligned} \overline{U}\frac{\partial \overline{T}}{\partial \overline{R}} + \overline{W}\frac{\partial \overline{T}}{\partial \overline{Z}} = &\frac{k}{\rho c_p \Omega L^2}\left(\frac{\partial^2 \overline{T}}{\partial \overline{R^2}} + \frac{1}{\overline{R}}\frac{\partial \overline{T}}{\partial \overline{R}} + \frac{\partial^2 \overline{T}}{\partial \overline{Z^2}}\right) + \frac{16\sigma^* T_\infty^3}{3\rho c_p \Omega k^* L^2}\frac{\partial^2 \overline{T}}{\partial \overline{Z^2}}\\ &+ \frac{D k_T(C_w - C_\infty)}{c_s c_p \Omega L^2 (T_w - T_\infty)}\left(\frac{\partial^2 \overline{C}}{\partial \overline{R^2}} + \frac{1}{\overline{R}}\frac{\partial \overline{C}}{\partial \overline{R}} + \frac{\partial^2 \overline{C}}{\partial \overline{Z^2}}\right) + \frac{\sigma B_0^2 \Omega L}{\rho c_p (T_w - T_\infty)}\frac{\overline{U^2}}{\overline{R}} + \frac{Q}{\rho c_p \Omega}\overline{T}, \end{aligned} \tag{16}$$

$$\overline{U}\frac{\partial \overline{C}}{\partial \overline{R}}+\overline{W}\frac{\partial \overline{C}}{\partial \overline{Z}}=\frac{D}{\Omega L^2}\left(\frac{\partial^2 \overline{C}}{\partial \overline{R^2}}+\frac{1}{\overline{R}}\frac{\partial \overline{C}}{\partial \overline{R}}+\frac{\partial^2 \overline{C}}{\partial \overline{Z^2}}\right)+\frac{Dk_T(T_w-T_\infty)}{T_m\Omega L^2(C_w-C_\infty)}\left(\frac{\partial^2 \overline{T}}{\partial \overline{R^2}}+\frac{1}{\overline{R}}\frac{\partial \overline{T}}{\partial \overline{R}}+\frac{\partial^2 \overline{T}}{\partial \overline{Z^2}}\right)-\frac{\overline{k}}{\Omega L^2}\overline{C}. \tag{17}$$

The boundary conditions (8) are reduced to

$$\begin{aligned}&\overline{Z}=0: \quad \overline{U}=\frac{2-\xi}{\xi}\overline{\lambda}\frac{\partial \overline{U}}{\partial \overline{Z}},\ \ \overline{V}=\overline{R}+\frac{2-\xi}{\xi}\overline{\lambda}\frac{\partial \overline{V}}{\partial \overline{Z}},\ \ \overline{W}=\frac{w_0}{\Omega L},\ \ \overline{T}=1,\ \ \overline{C}=1,\\ &\overline{Z}\to\infty: \quad \overline{U}\to 0,\overline{V}\to 0,\quad \overline{T}\to 0,\quad \overline{C}\to 0,\ \ \overline{P}\to 0.\end{aligned} \tag{18}$$

The governing equations are obtained by introducing a dimensionless normal distance from the disk, $\eta=\overline{Z}/\sqrt{\overline{\nu}}$ along with the von-Karman transformations,

$$\begin{aligned}&\overline{U}=\overline{R}F(\eta),\quad \overline{V}=\overline{R}G(\eta),\quad \overline{W}=\sqrt{\overline{\nu}}H(\eta).\\ &\overline{T}=\theta(\eta),\quad \overline{C}=\varphi(\eta),\quad \overline{P}=\overline{\nu}\overline{P}(\eta)\end{aligned} \tag{19}$$

Where F, G, H, θ, φ and $\overline{P}$ are non-dimensionless functions in terms of vertical co-ordinate η. Substituting these transformations into Eqs. (12)–(17) gives the nonlinear ordinary differential equations, expressed as

$$2F+H^{/}=0, \tag{20}$$

$$F^{//}-HF^{/}-F^2+G^2-(M+S)F+\alpha\theta+N\varphi=0, \tag{21}$$

$$G^{//}-HG^{/}-2FG-(M+S)G=0, \tag{22}$$

$$H^{//}-HH^{/}-\overline{P^{/}}=0, \tag{23}$$

$$\frac{1}{P_r}\left(1+\frac{4}{3R_d}\right)\theta^{//}-H\theta^{/}+D_u\varphi^{//}+JF^2+\delta\theta=0, \tag{24}$$

$$\frac{1}{S_c}\varphi^{//}-H\varphi^{/}+S_0\theta^{//}-\beta\varphi=0. \tag{25}$$

With the appropriate boundary conditions:

$$\begin{aligned}&\eta=0; F(0)=\gamma F^{/}(0),\ \ G(0)=1+\gamma G^{/}(0), H(0)=W_s,\ \ \theta(0)=1,\ \ \varphi(0)=1,\\ &\eta\to\infty; F(\infty)=0, G(\infty)=0,\ \ \theta(\infty)=0,\ \ \varphi(\infty)=0, \overline{P}(\infty)=0.\end{aligned} \tag{26}$$

Where $\gamma=\left[(2-\xi)\lambda\sqrt{\Omega}\right]/\xi\sqrt{\nu}$ the slip is factor and $W_s=w_0/\sqrt{\nu\,\Omega}$ represents a uniform suction $(W_s<0)$ at the disk surface. The boundary conditions given by Eq. (26) imply that the radial (F), the tangential (G) components of velocity, temperature and concentration vanish sufficiently far away from the disk, whereas the axial velocity component (H) is anticipated to approach a yet unknown asymptotic limit for sufficiently large η-values.

3. Skin-friction coefficient, Nusselt number and Sherwood number

The parameters of engineering interest for the present problem are the local skin-friction coefficients and the local rates of heat and mass transfer to the surface are calculated. The radial shear stress and tangential shear stress are given by:

$$\tau_{\varphi z} = \mu \left(\frac{\partial v}{\partial z} + \frac{1}{r} \frac{\partial w}{\partial \varphi} \right)_{z=0},$$

$$\tau_{zr} = \mu \left(\frac{\partial u}{\partial z} + \frac{\partial w}{\partial r} \right)_{z=0},$$

The tangential and radial skin-friction coefficient are, respectively, given by, Eq. (27):

$$\begin{aligned} C_{f_1} &= \tau_{\varphi z} / \rho \Omega^2 L^2 = \sqrt{R_e}\, G^{/}(0), \\ C_{f_2} &= \tau_{zr} / \rho \Omega^2 L^2 = \sqrt{R_e}\, F^{/}(0), \end{aligned} \tag{27}$$

Now the heat flux (q_w) and the mass flux (J_w) at the surface are given by.

$$q_w = -k \left(\frac{\partial T}{\partial z} \right)_{z=0}, \text{ and } M_w = -D \left(\frac{\partial C}{\partial z} \right)_{z=0}.$$

Hence the Nusselt number, N_u and Sherwood number, S_h are obtained as Eqs. (28) and (29), respectively:

$$N_u = \frac{L q_w}{k (T_w - T_\infty)(\overline{\nu})^{-1/2}} = -\theta^{/}(0), \tag{28}$$

And

$$S_h = \frac{L M_w}{D (C_w - C_\infty)(\overline{\nu})^{-1/2}} = -\varphi^{/}(0). \tag{29}$$

Where $R_e = \overline{R^2}/\overline{\nu}$ is the rotational Reynolds number.

4. Numerical results and discussion

The system of non-linear ordinary differential Eqs. (20)–(25) together with the boundary conditions (26) are locally similar and solved numerically by using the Keller-box method. In order to gain physical insight, the velocity (radial, axial and tangential), temperature, concentration and pressure profiles have been discussed by assigning numerical values to the parameter, encountered in the problem which the numerical results are tabulated and displayed with the graphical illustrations.

In order to verify the accuracy of our present method, we have compared our results with those of Frusteri and Osalusi [15], Osalusi and Sibanda [23] and Maleque and Sattar [24]. **Table 1** shows the values of $F^{/}(0)$, $-G^{/}(0)$ and $-\theta^{/}(0)$ for various values of W_s. The comparisons in all above cases are found to be excellent and agreed, so it is good.

Figures 2, **3** and **11a–d** display the velocity (radial, axial and tangential), temperature, concentration and pressure profiles under the magnetic field parameter, porosity parameter and Schmidt number. The (radial, axial and tangential) components of the velocity and pressure profile decrease with increase of magnetic field due to the inhibiting influence of the Lorentz force and increasing of all porosity parameter and Schmidt number, while the temperature and the concentration profiles increase with increasing of all magnetic field parameter, porosity parameter and Schmidt number. In **Figures 4** and **5a–d**, it is clear that the (radial and axial)

W_s	$F'(0)$				$-G'(0)$				$-\theta'(0)$			
	Frusteri et al. [15]	**Osalusi et al. [23]**	**Maleque et al. [24]**	**Present study**	**Frusteri et al. [15]**	**Osalusi et al. [23]**	**Maleque et al. [24]**	**Present study**	**Frusteri et al. [15]**	**Osalusi et al. [23]**	**Maleque et al. [24]**	**Present study**
	$\gamma = 0, \varepsilon = 0$											
0.0	0.4241	0.4241	0.5102	0.4627	0.6514	0.6514	0.6160	0.6241	0.5387	0.5387	0.3258	0.3171
−2.0	0.2324	0.2324	0.2425	0.2435	2.0687	2.0687	2.0391	2.0452	1.5196	1.5196	1.4421	1.4746
−4.0	0.1246	0.1246	0.1248	0.1245	4.0065	4.0065	4.0054	4.0052	2.8520	2.8520	2.8447	2.8432
−5.0	0.0999	0.0999	0.0999	0.0998	5.0029	5.0029	5.0031	5.0032	3.5541	3.5541	3.5541	3.5539
−10.0	0.0499	0.0499	0.0506	0.0502	10.0003	10.0003	10.0017	10.0019	7.1002	7.1002	7.1020	7.1018

Table 1.
Comparison of the current and recent numerical values of the radial and tangential skin-friction coefficients and the rate of heat transfer coefficient for various of W_s with $S = 0.0, \alpha = 0.0, N = 0.0, J = 0.0, \delta = 0.0, P_r = 0.71, \beta = 0.0, R_d = 10^9, D_u = 0.0, S_0 = 0.0, S_c = 1.0$ and $M = 0$.

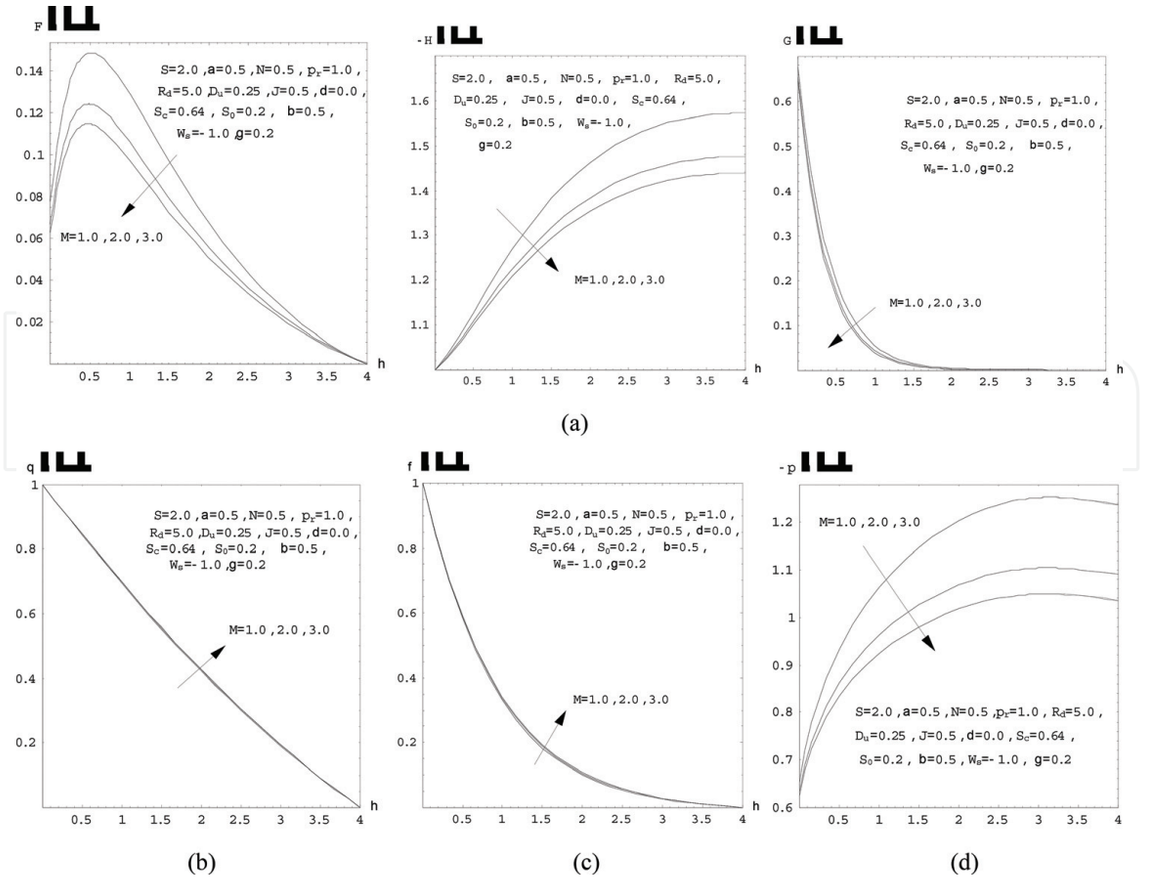


Figure 2.
Effect of magnetic field parameter on (a) the velocity (radial, axial and tangential) profile, (b) the temperature profile, (c) the concentration and (d) the pressure profile.

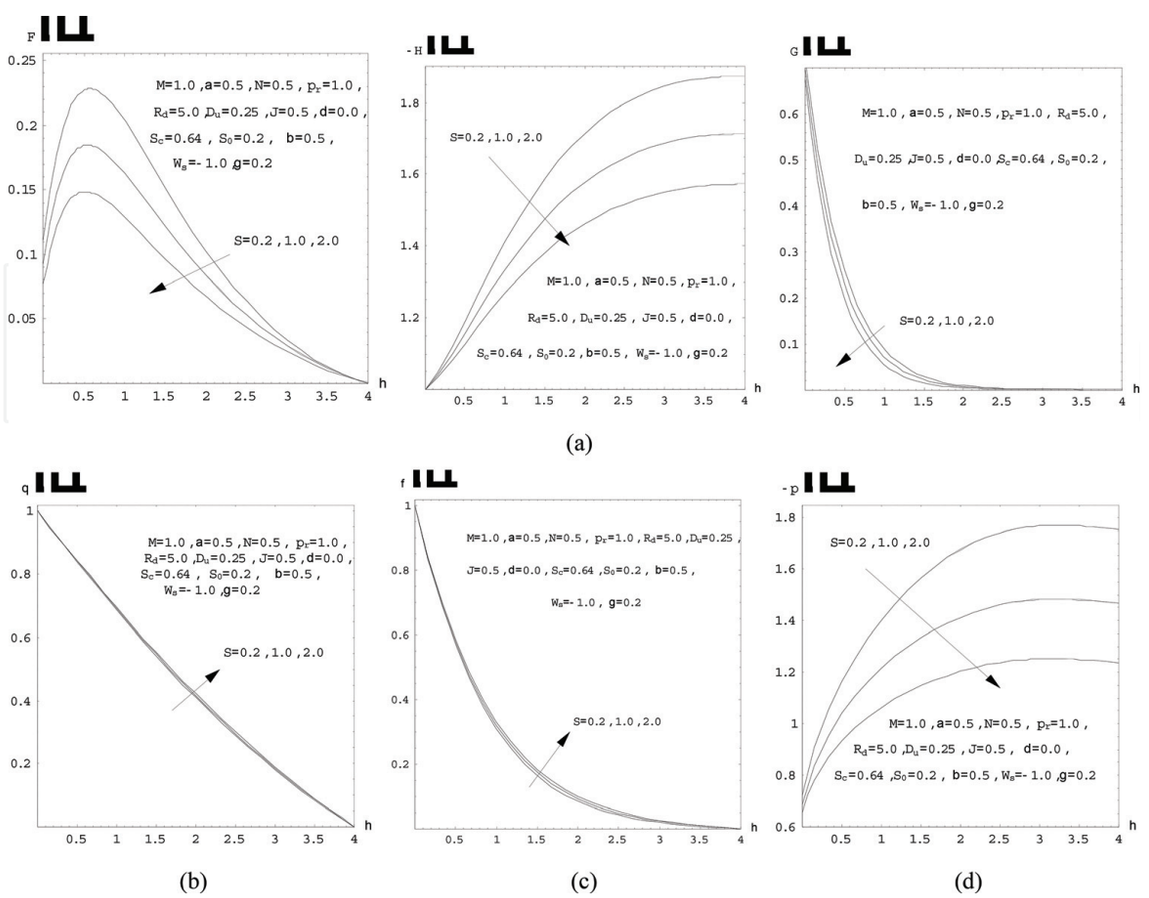


Figure 3.
Effect of porosity parameter on (a) the velocity (radial, axial and tangential) profile, (b) the temperature profile, (c) the concentration and (d) the pressure profile.

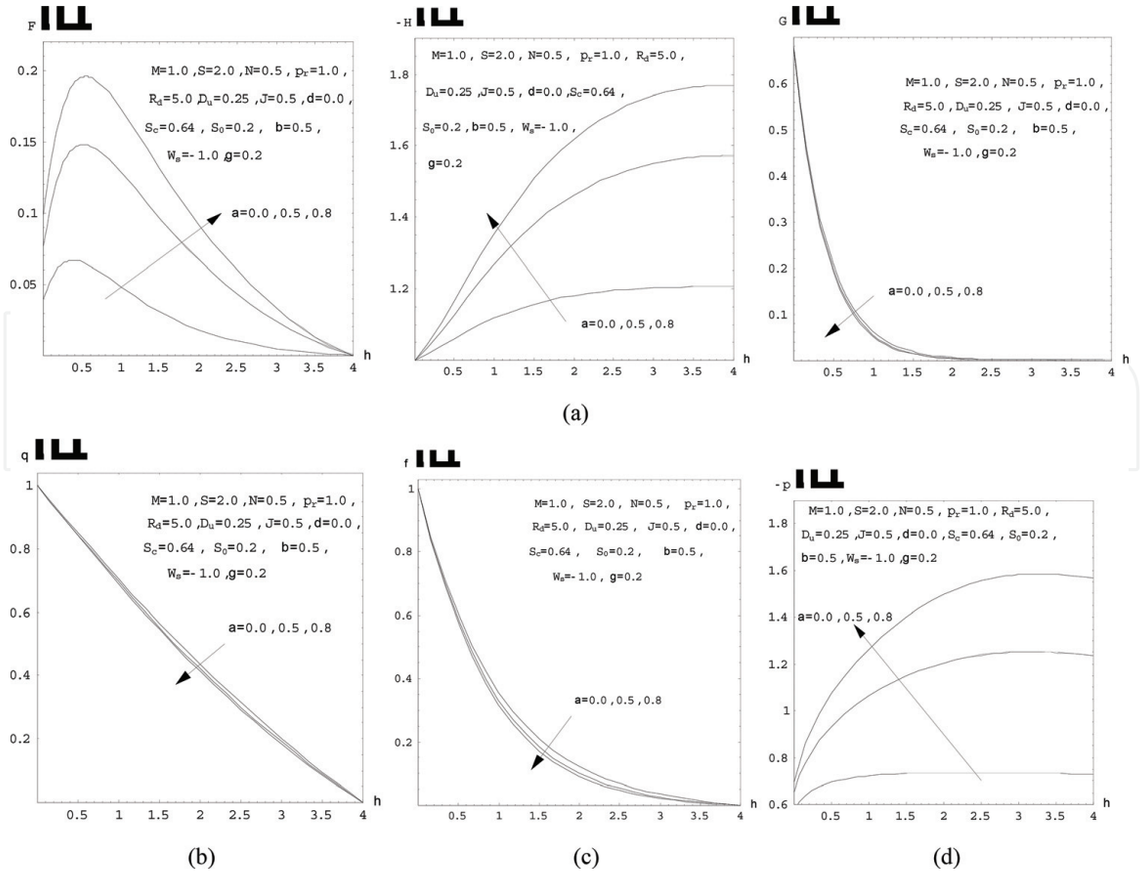


Figure 4.
Effect of temperature buoyancy parameter on (a) the velocity (radial, axial and tangential) profile, (b) the temperature profile, (c) the concentration and (d) the pressure profile.

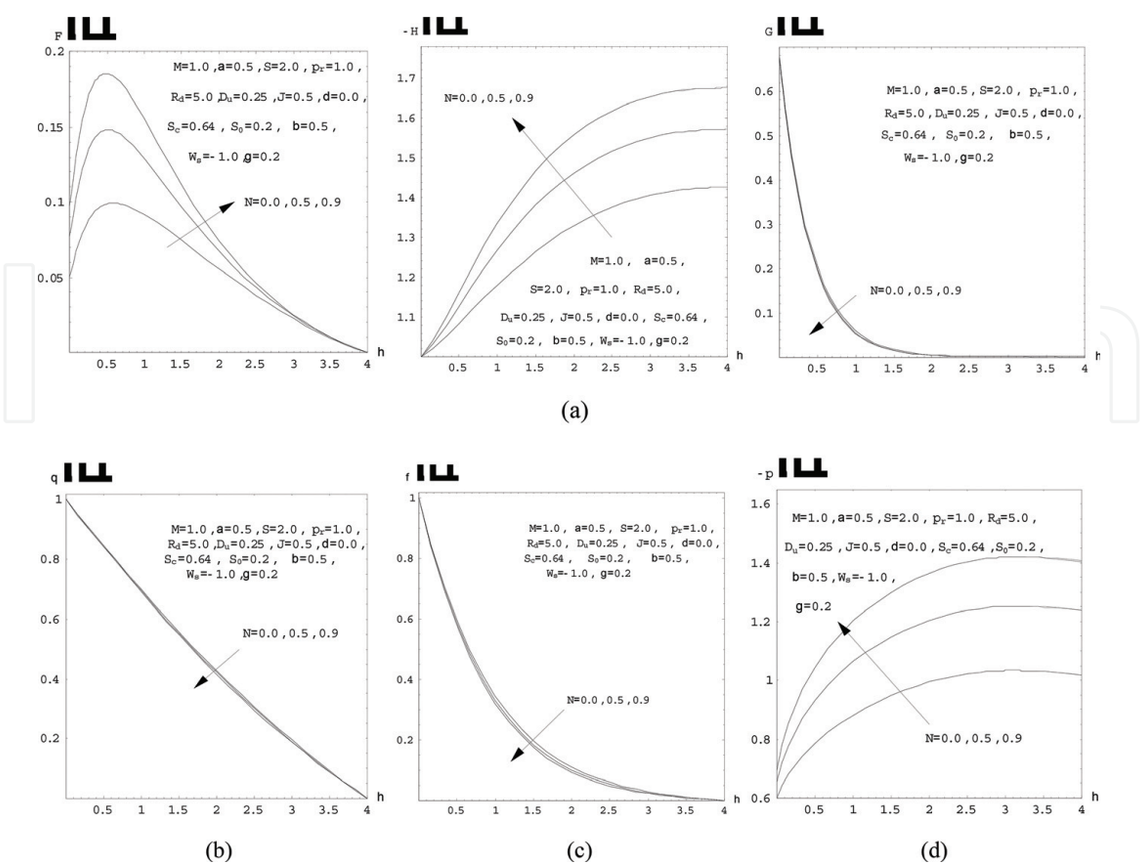


Figure 5.
Effect of concentration buoyancy parameter on (a) the velocity (radial, axial and tangential) profile, (b) the temperature profile, (c) the concentration and (d) the pressure profile.

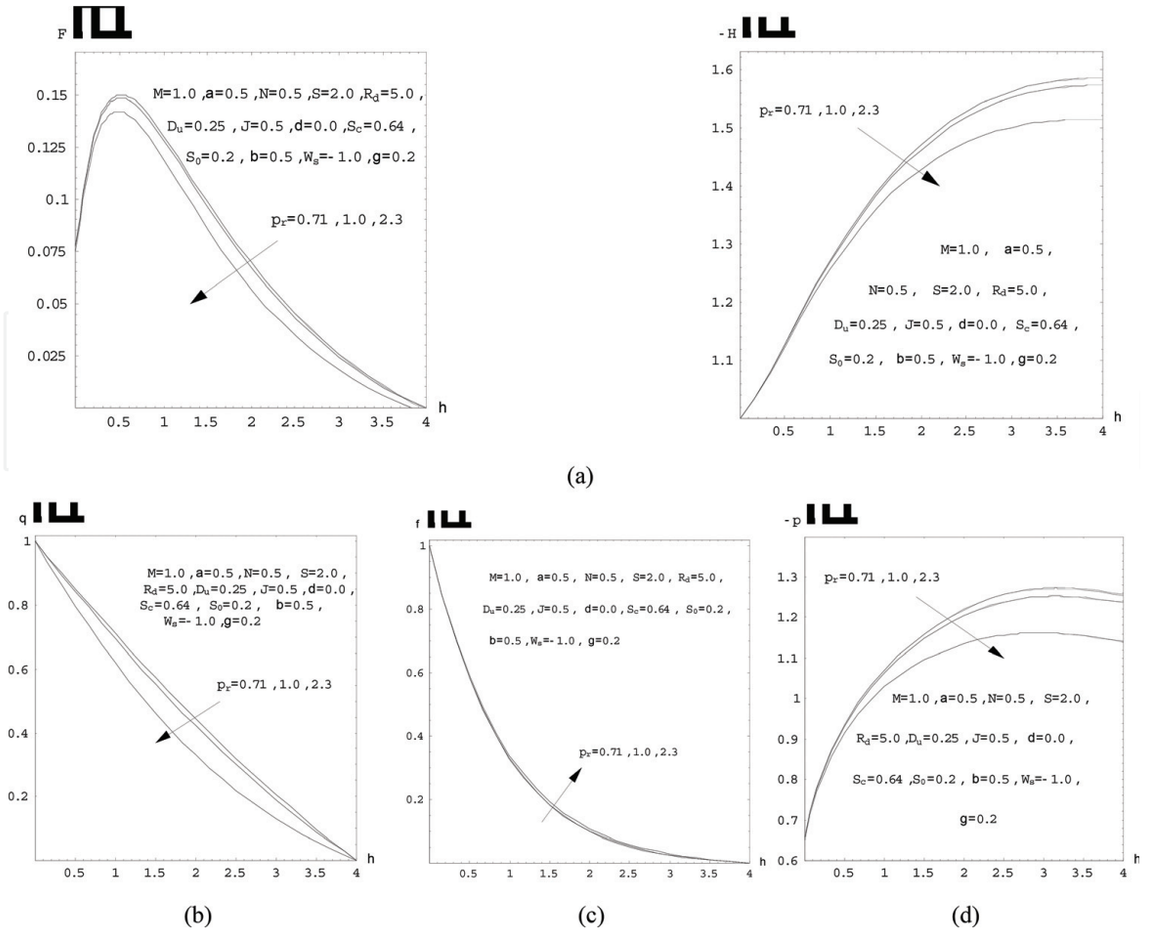


Figure 6.
Effect of Prandtl number on (a) the velocity (radial and axial) profile, (b) the temperature profile, (c) the concentration and (d) the pressure profile.

components of the velocity and pressure profiles increase with increase of temperature buoyancy parameter and increasing concentration buoyancy parameter, while the tangential component of the velocity, the temperature and the concentration profiles decrease with increasing temperature buoyancy parameter and concentration buoyancy parameter.

The effects of P_r on the (radial and axial) components of the velocity, the temperature, concentration and pressure profiles are shown in **Figure 6a–d**, respectively. It is observed that both the (radial and axial) components of the velocity, the temperature and pressure profiles decrease with the increase of Prandtl number. While, the concentration profile increase. Physically, it means that thermal boundary layer thickness gets decreased. In fact, it is well known that the thermal boundary layer thickness is inversely proportional to the square root of Prandtl number. Hence, the decrease of temperature profile with increasing P_r is straightforward.

Figures 7 and **10a–d** show the effects of radiation parameter and heat source parameter on the velocity (radial and axial), temperature, concentration and pressure profiles, also, we found that the (radial and axial) components of the velocity, temperature and pressure profiles increase with the increase of radiation parameter and increasing heat source parameter. While the concentration profile decrease. The effects of D_u and S_0 on the velocity (radial and axial), temperature, concentration and pressure profiles, are shown in **Figure 8a–d**, respectively. It is observed that the (radial and axial) components of the velocity, temperature, concentration and pressure profiles increase with the decreasing the Dufour's number and increasing Soret number.

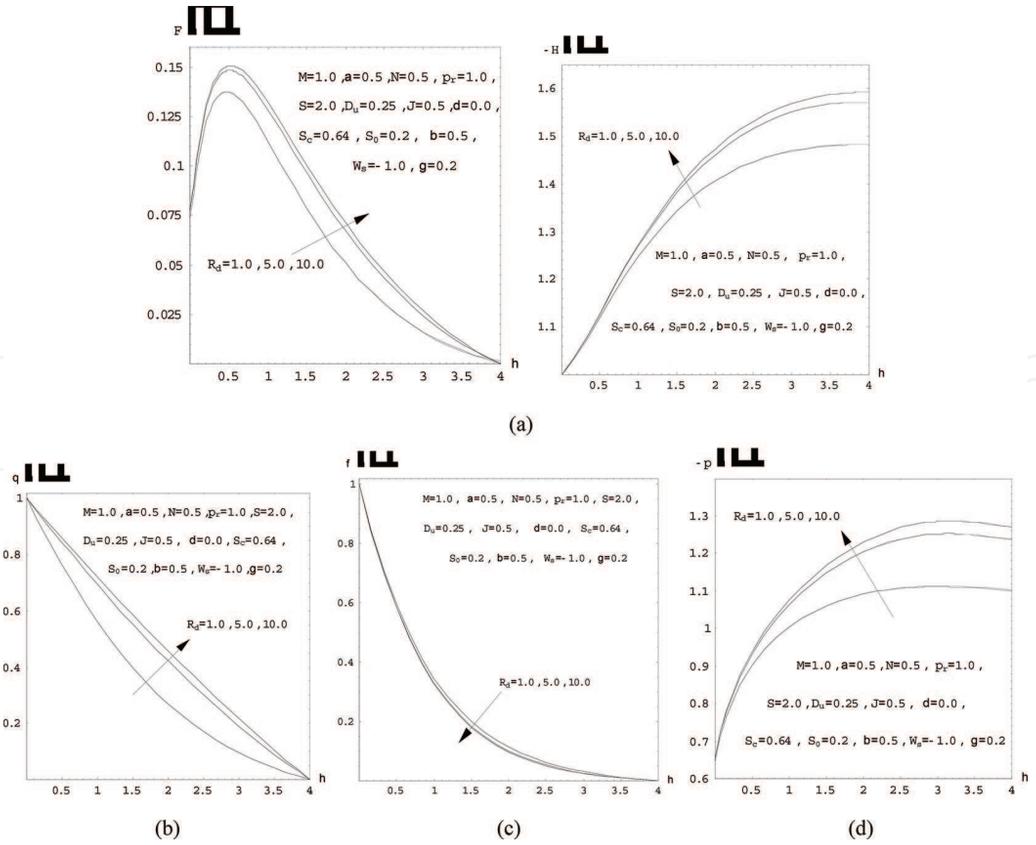


Figure 7.
Effect of radiation parameter on (a) the velocity (radial and axial) profile, (b) the temperature profile, (c) the concentration and (d) the pressure profile.

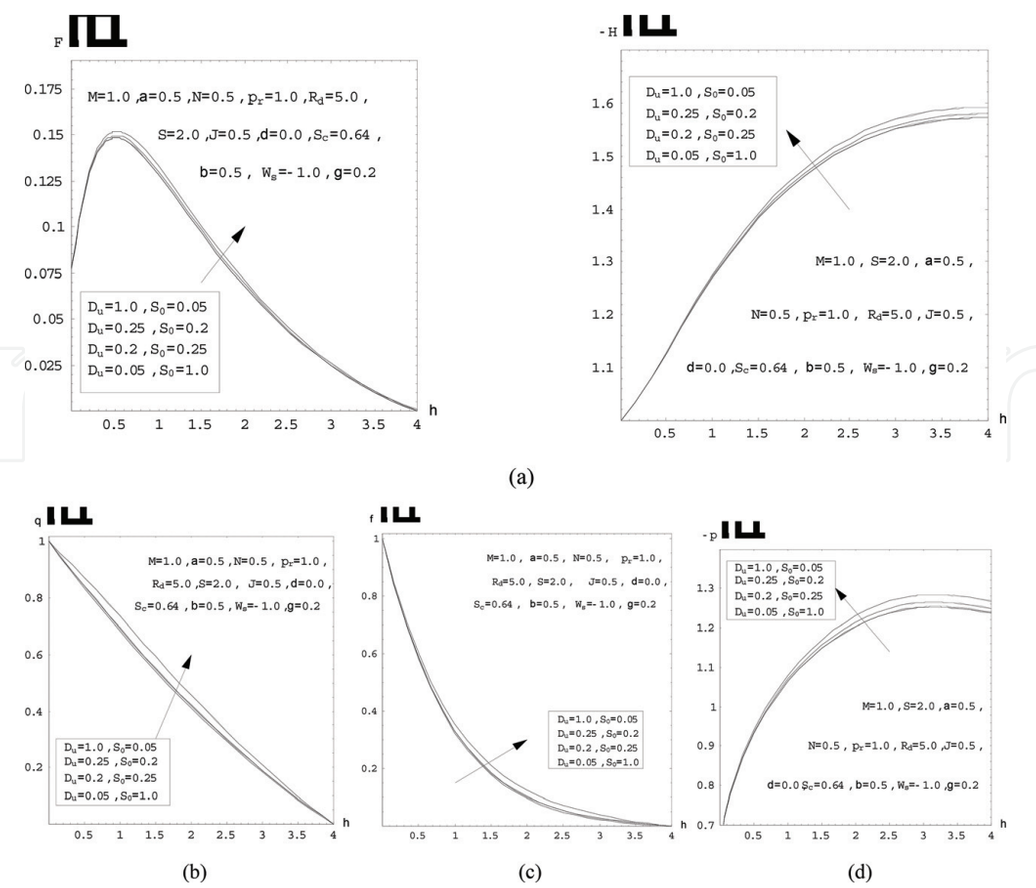


Figure 8.
Effect of Soret and Dufour's number on (a) the velocity (radial and axial) profile, (b) the temperature profile, (c) the concentration and (d) the pressure profile.

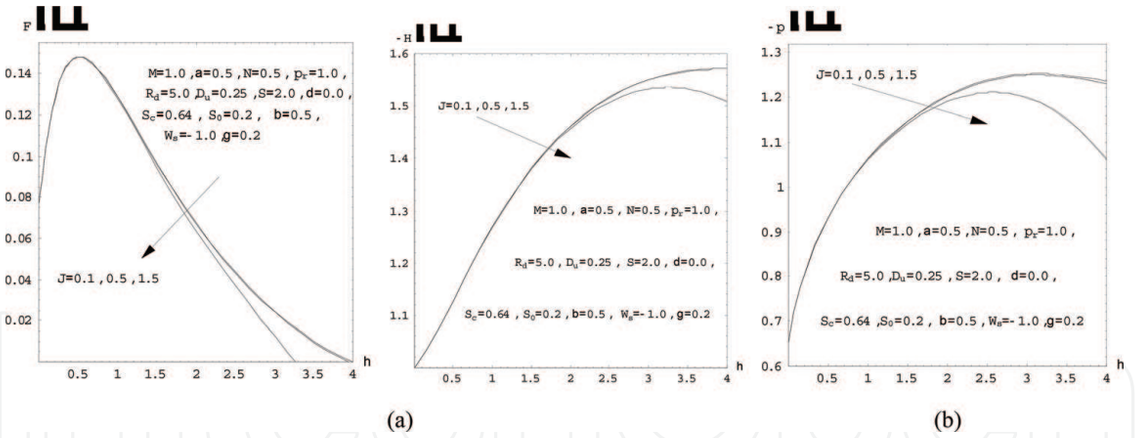


Figure 9.
Effect of Joule heating parameter on (a) the velocity (radial and axial) profile, and (b) the pressure profile.

The effects of *J* on the velocity (radial and axial) and pressure profiles, are shown in **Figure 9a** and **b**, respectively. We found that the (radial and axial) components of the velocity and pressure profiles decrease with the increase Joule heating parameter. In **Figure 12a–c**, it is clear that the (radial and axial) components of the velocity, concentration and pressure profiles decrease with increase of chemical reaction parameter. **Figure 13a–d** displays the velocity (radial, axial and tangential), temperature, concentration and pressure profiles under the suction

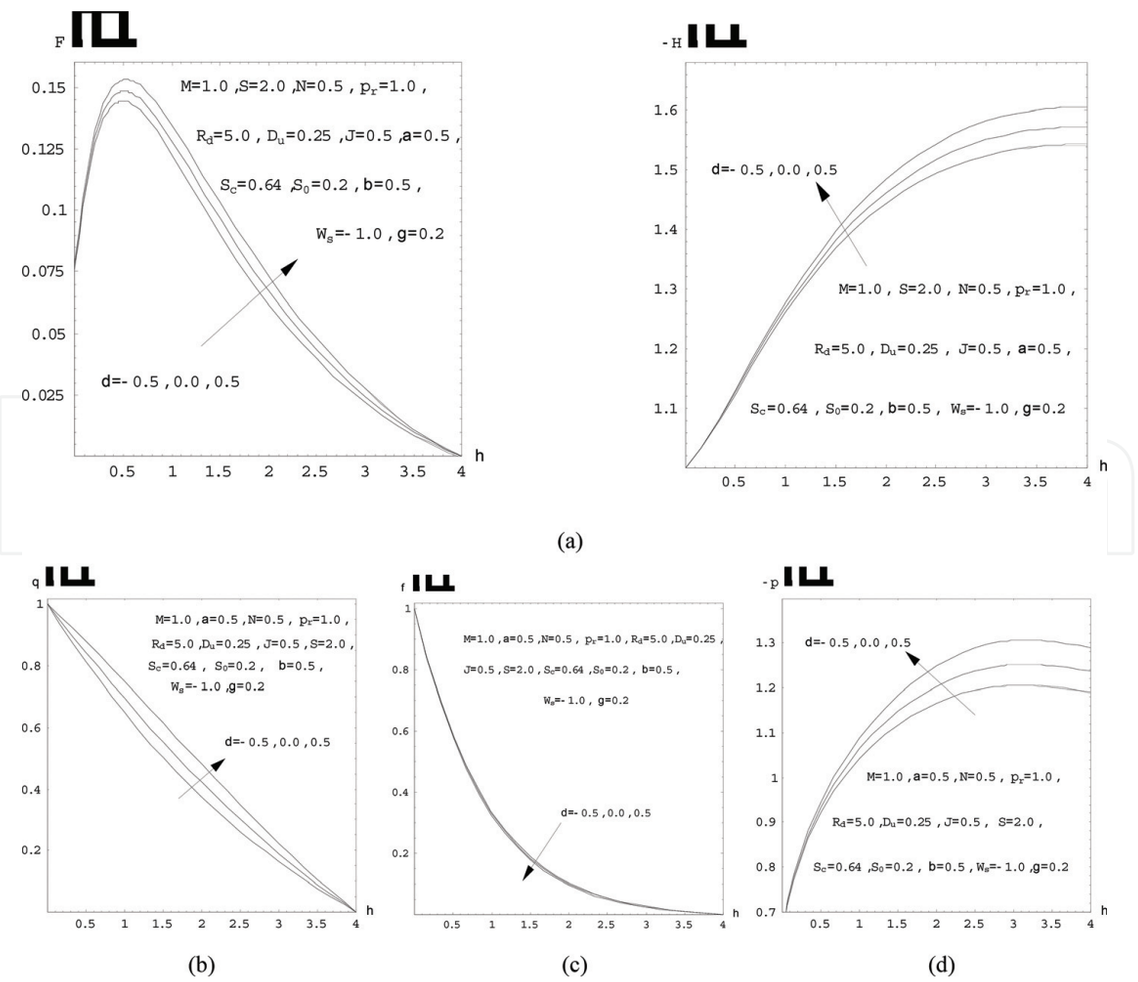


Figure 10.
Effect of heat source parameter on (a) the velocity (radial and axial) profile, (b) the temperature profile, (c) the concentration and (d) the pressure profile.

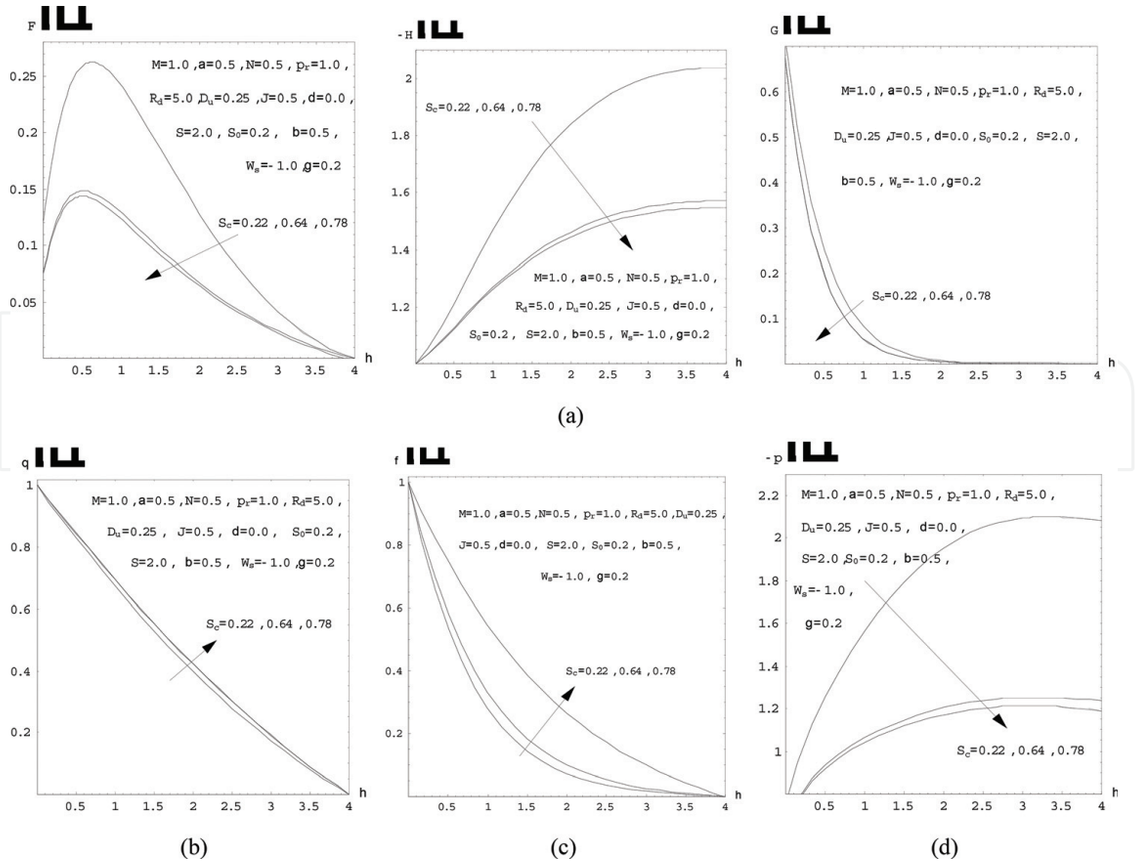


Figure 11.
Effect of Schmidt number on (a) the velocity (radial, axial and tangential) profile, (b) the temperature profile, (c) the concentration and (d) the pressure profile.

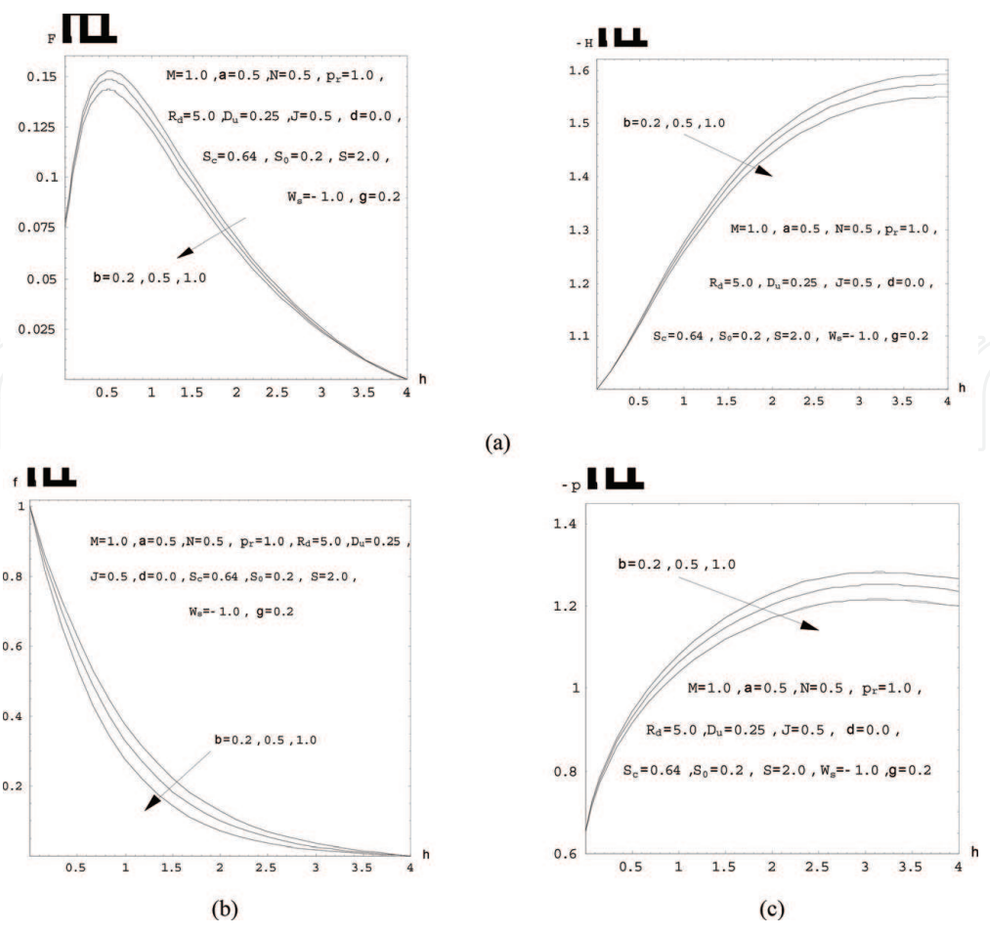


Figure 12.
Effect of chemical reaction parameter on (a) the velocity (radial and axial) profile, (b) the concentration and (c) the pressure profile.

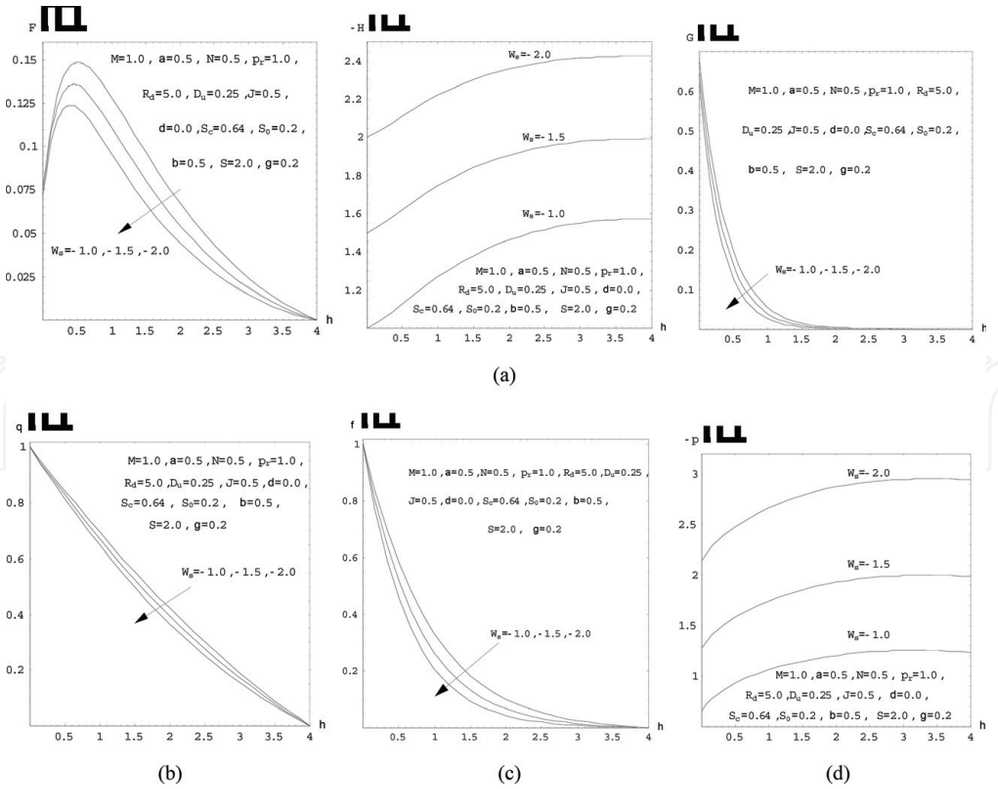


Figure 13.
Effect of suction parameter on (a) the velocity (radial, axial and tangential) profile, (b) the temperature profile, (c) the concentration and (d) the pressure profile.

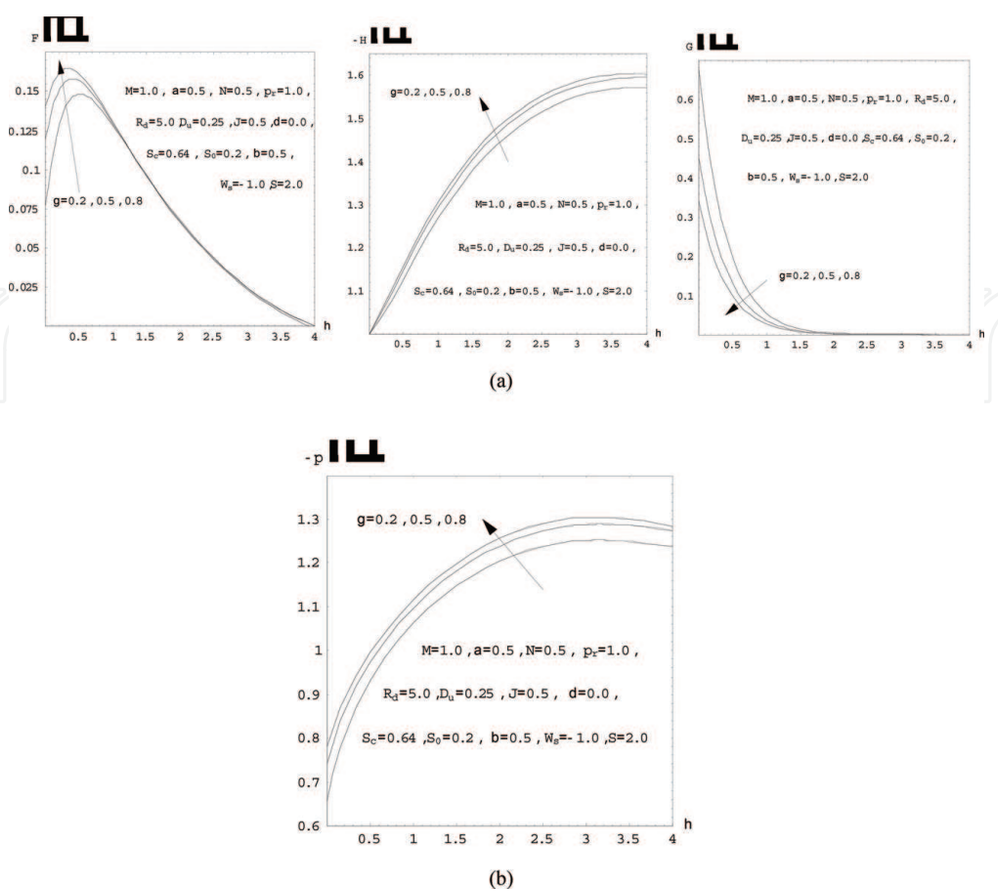


Figure 14.
Effect of slip parameter on (a) the velocity (radial, axial and tangential) profile, and (b) the pressure profile.

M	S	α	N	P_r	R_d	D_u&S_0	J	δ	S_c	β	W_s	γ	$R_e^{-1/2}C_{f1}$	$-R_e^{-1/2}C_{f2}$	$-N_u$	$-S_h$
0.1	2.0	0.5	0.5	1.0	5.0	0.25 & 0.2	0.5	0.0	0.64	0.5	−1.0	0.2	0.3857	1.6257	0.3144	1.0486
2.0													0.3323	1.7275	0.3116	1.0367
3.0													0.3112	1.7732	0.3105	1.0319
0.1	0.2												0.5534	1.3978	0.3220	1.0870
	1.0												0.4629	1.5071	0.3185	1.0663
	2.0												0.3857	1.6257	0.3144	1.0486
0.1	2.0	0.0											0.1970	−1.6005	0.3039	1.0056
		0.5											0.3857	1.6257	0.3144	1.0486
		0.8											0.4953	1.6397	0.3198	1.0725
0.1	2.0	0.5	0.0										0.2510	1.6096	0.3093	1.0247
			0.5										0.3857	1.6257	0.3144	1.0486
			0.9										0.4894	1.6377	0.3180	1.0667
0.1	2.0	0.5	0.5	0.71									0.3879	1.6261	0.2944	1.0522
				1.0									0.3857	1.6257	0.3144	1.0486
				2.3									0.3757	1.6241	0.4155	1.0326
0.1	2.0	0.5	0.5	1.0	1.0								0.3683	1.6229	0.5022	1.0194
					5.0								0.3857	1.6257	0.3144	1.0486
					10.0								0.3892	1.6263	0.2828	1.0541
0.1	2.0	0.5	0.5	1.0	5.0	1.0 & 0.05							0.3910	1.6266	0.2324	1.0591
						0.25 & 0.2							0.3857	1.6257	0.3144	1.0486
						0.2 & 0.25							0.3856	1.6256	0.3195	1.0454
0.1	2.0	0.5	0.5	1.0	5.0	0.25 & 0.2	0.1						0.3858		0.3157	1.0487

M	S	α	N	P_r	R_d	D_u&S_0	J	δ	S_c	β	W_s	γ	$R_e^{-1/2}C_{f1}$	$-R_e^{-1/2}C_{f2}$	$-N_u$	$-S_h$
							0.5						0.3857		0.3144	1.0486
							1.5						0.3854		0.3111	1.0485
0.1	2.0	0.5	0.5	1.0	5.0	0.25 & 0.2	0.5	−0.5					0.3795	1.6247	0.3938	1.0370
								0.0					0.3857	1.6257	0.3144	1.0486
								0.5					0.3931	1.6270	0.2239	1.0625
0.1	2.0	0.5	0.5	1.0	5.0	0.25 & 0.2	0.5	0.0	0.22				0.6083	1.4121	0.3451	0.5590
									0.64				0.3857	1.6257	0.3144	1.0486
									0.78				0.3777	1.6278	0.3084	1.2094
0.1	2.0	0.5	0.5	1.0	5.0	0.25 & 0.2	0.5	0.0	0.64	0.2			0.3927	1.6268	0.3193	0.9130
										0.5			0.3857	1.6257	0.3144	1.0486
										1.0			0.3770	1.6244	0.3075	1.2368
0.1	2.0	0.5	0.5	1.0	5.0	0.25 & 0.2	0.5	0.0	0.64	0.5	−1.0		0.3857	1.6257	0.3144	1.0486
											−1.5		0.3737	1.7684	0.3445	1.2854
											−2.0		0.3590	1.9095	0.3764	1.5404
0.1	2.0	0.5	0.5	1.0	5.0	0.25 & 0.2	0.5	0.0	0.64	0.5	−1.0	0.2	0.3857	1.6257	0.3144	1.0486
												0.5	0.2403	1.0968	0.3156	1.0573
												0.8	0.1757	0.8264	0.3162	1.0613

Table 2.
Numerical of the values skin-friction coefficient $\left(R_e^{-1/2}C_{f1}, -R_e^{-1/2}C_{f2}\right)$*, Nusselt number* N_u *and Sherwood number* S_h *at the surface with M, S,* α*, N,* P_r*,* R_d*,* D_u&S_0*, J,* δ*,* S_c*,* β*,* W_s*and* γ*.*

parameter. The (radial, axial and tangential) components of the velocity, temperature, concentration and pressure profiles decrease with increase of suction parameter. The effects of γ on the velocity (radial, axial and tangential) and pressure profiles are shown in **Figure 14a** and **b**, respectively. It is observed that the (radial and axial) components of the velocity, and pressure profiles increase with the increasing slip parameter. While the tangential component of the velocity profile decrease.

The radial and tangential skin frictions and the heat and mass transfer coefficients are tabulated in **Table 2** for various values of M, S, α, N, P_r, R_d, D_u&S_0, J, δ, S_c, β, W_s and γ. We observed that increase for all magnetic field parameter M and porosity parameter S leads to an decrease in the all tangential skin friction $\left(-G^{/}(0)\right)$, heat transfer rate $\left(-\theta^{/}(0)\right)$ and mass transfer rate $\left(-\varphi^{/}(0)\right)$, while an increase in the radial skin friction $\left(F^{/}(0)\right)$, the increase for all radial skin friction, tangential skin friction, heat transfer rate and mass transfer rate, with increasing of the temperature buoyancy parameter α and the concentration buoyancy parameter N. We found that the radial skin friction, tangential skin friction, mass transfer rate decreases while heat transfer rate increase with increasing of Prandtl number, Dufour number decreases and Soret number increases. It can that be seen that the radial skin friction, tangential skin friction and mass transfer rate increase while heat transfer rate decrease with increasing values of R_d and δ. It is observed that an increase in the Joule heating parameter, results in a decrease in the tangential Skin-friction coefficient, Nusselt number and Sherwood number. The tangential skin friction and heat transfer rate decrease but the radial skin friction and mass transfer rate increase with increasing the Schmidt number. It also can be seen from this table that increasing the chemical reaction parameter to decrease in the radial skin friction, tangential skin friction and heat transfer rate while increase the mass transfer rate. We found also the tangential skin friction increase but the radial skin friction, Nusselt number and Sherwood number decrease with increasing the suction parameter. Finally, the radial skin friction and the tangential skin friction decrease but Nusselt number and Sherwood number increase with increasing slip parameter.

5. Conclusions

In this work, thermal radiation and thermal diffusion effects over an electrically conducting, Newtonian fluid in a steady laminar magnetohydrodynamic convective flow over a porous rotating infinite disk with the consideration of heat and mass transfer in the presence of Soret and Dufour's diffusion effects have been obtained and studied numerically. Magnetic field parameter, porosity parameter, temperature buoyancy parameter, concentration buoyancy parameter, Prandtl number, radiation parameter, Soret and Dufour's number, Joule heating parameter, heat source parameter, Schmidt number, chemical reaction parameter, suction parameter, slip parameter effects were considered in the separate cases. The subsequent outcome may be drawn as:

1. The components (radial, axial and tangential) of the velocity, temperature, concentration and pressure profiles under the porosity parameter. The (radial, axial and tangential) components of the velocity and pressure profile decrease with increasing porosity parameter, while the temperature and the concentration profiles increase with increasing porosity parameter. And also, that increase porosity parameter S leads to a decrease in the all tangential skin

friction $\left(-G^{/}(0)\right)$, heat transfer rate $\left(-\theta^{/}(0)\right)$ and mass transfer rate $\left(-\varphi^{/}(0)\right)$, while an increase in the radial skin friction $\left(F^{/}(0)\right)$.

2. The (radial and axial) components of the velocity and pressure increase with increasing of temperature buoyancy parameter and concentration buoyancy parameter, while the tangential component of the velocity, the temperature and the concentration profiles decrease with increasing temperature buoyancy parameter and concentration buoyancy parameter. We found that the increase for all radial skin friction, tangential skin friction, heat transfer rate and mass transfer rate, with increasing of the temperature buoyancy parameter α and the concentration buoyancy parameter N.

3. The (radial and axial) components of the velocity, temperature and pressure profiles increase with the increase of heat source parameter. While the concentration profile decrease. And also, the radial skin friction, tangential skin friction and mass transfer rate increase while heat transfer rate decrease with increasing value of δ.

4. The (radial and axial) components of the velocity, concentration and pressure profiles decrease with increase of chemical reaction parameter. And in **Table 2**, an increase the chemical reaction parameter, results in an decrease in the (radial and tangential) Skin-friction coefficient and Nusselt number, while Sherwood number increases.

Nomenclature

B	external uniform magnetic field
B_0	constant magnetic flux density
b	induced magnetic field
C	concentration distribution
C_w	uniform concentration
C_∞	constant concentration
c_p	specific heat at constant pressure
c_s	concentration susceptibility
C_{f1}	tangential skin-friction coefficient
C_{f2}	radial skin-friction coefficient
D	molecular diffusion coefficient
D_u	Dufour number $\left[= Dk_T(C_w - C_\infty)/\nu c_s c_p(T_w - T_\infty)\right]$
g	gravitational acceleration, $[\mathrm{m\ s^{-2}}]$
k	thermal conductivity
k_1	rate of chemical reaction
K_T	thermal-diffusion rate
K_1^*	permeability of the porous medium
k^*	Rosseland mean absorption coefficient
F, G, H	radial (F), tangential (G) and axial (H) components of dimensionless velocity
M	magnetic field parameter $\left[= \sigma B_0^2/\rho\Omega\right]$
N	concentration buoyancy parameter $\left[= g\beta_c(C_w - C_\infty)/L\overline{R}\Omega^2\right]$
N_u	Nusselt number
n	normal direction to the wall

$\vec{J}$	electric current density
J	Joule heating parameter $\left[= \sigma B_0^2 \Omega L/\rho c_p (T_w - T_\infty)\right]$
P_r	Prandtl number $\left[= \nu\rho c_p/k\right]$
p	pressure distribution, [N m^{-2}]
p_∞	constant pressure
Q	volumetric heat generation/absorption rate, [W m^{-3}]
q_r	radiative heat flux, [W m^{-2}]
R_d	radiation parameter $\left[= k^* k/4\sigma^* T_\infty^3\right]$
S	porosity parameter $\left[= \overline{\nu}/\overline{k_1}\right]$
S_0	Soret number $[= Dk_T(T_w - T_\infty)/\nu T_m(C_w - C_\infty)]$
S_c	Schmidt number $[= \nu/D]$
S_h	Sherwood number
T	temperature distribution [K]
T_m	mean fluid temperature [K]
T_w	uniform temperature [K]
T_∞	constant temperature [K]
(u, v, w)	components of the flow velocity are in the directions of increasing (r, φ, z), respectively, [m s^{-1}]
U_t	tangential velocity, [m s^{-1}]
w_0	uniform suction
Greek symbols	
μ_m	magnetic permeability, [kg m^{-1} s^{-1}]
ξ	tangent momentum accommodation coefficient
λ	mean free path
ρ	fluid density, [kg m^{-3}]
μ	dynamic viscosity, [kg m^{-1} s^{-1}]
ν	kinematic viscosity of the ambient fluid, [m^2 s^{-1}]
δ	heat source parameter $\left[= Q/\Omega\rho c_p\right]$
α	temperature buoyancy parameter $\left[= g\beta_T(T_w - T_\infty)/L\overline{R}\Omega^2\right]$
γ	slip factor
η	similarity variable
θ	dimensionless temperature distribution
φ	dimensionless concentration distribution
σ	electrical conductivity
σ	Stephan-Boltzmann constant
Ω	constant angular velocity
β	chemical reaction parameter $\left[= \overline{k}/\Omega L^2\right]$
β_T	coefficient of temperature
β_C	coefficient of concentration
Subscripts	
w, ∞	conditions at the surface and in the free stream

DOI: http://dx.doi.org/10.5772/intechopen.82186

IntechOpen

IntechOpen

Author details

Gamal M. Abdel-Rahman[1*] and Faiza M.N. El-fayez[2]

1 Department of Mathematics, Faculty of Science, Benha University, Benha, Egypt

2 Mathematical Science Department, College of Sciences, Princess Nourah Bint Abdulrahman University, Riyadh, KSA

*Address all correspondence to: gamalm60@yahoo.com

IntechOpen

© 2019 The Author(s). Licensee IntechOpen. This chapter is distributed under the terms of the Creative Commons Attribution License (http://creativecommons.org/licenses/by/3.0), which permits unrestricted use, distribution, and reproduction in any medium, provided the original work is properly cited. CC BY

References

[1] Von Karman T. Uber laminare und turbulente Reibung. Zeitschrift für Angewandte Mathematik und Mechanik. 1921;**1**:1233-1255

[2] Cochran WG. The flow due to a rotating disk. Proceedings of the Cambridge Philosophical Society. 1934; **30**:365-375

[3] Benton ER. On the flow due to a rotating disk. Journal of Fluid Mechanics. 1966;**24**:781-800

[4] Nield DA, Bejan A. Convection in Porous Media. 2nd ed. New York: Springer-Verlag; 1999

[5] Eckert ERG, Drake RM. Analysis of Heat and Mass Transfer. New York: McGraw-Hill; 1972

[6] Northrup EF. Some newly observed manifestations of forces in the interior of an electrical conductor. Physics Review. 1907;**24**:474-497

[7] Tillack MS, Morley NB. Magnetohydrodynamics. Standard Handbook for Electrical Engineer. McGraw Hill; 1998

[8] Hayat T, Nadeem S, Siddiqui A, Asghar S. An oscillating hydromagnetic non-Newtonian flow in a rotating system. Applied Mathematics Letters. 2004;**17**:609-614

[9] Ahn CH, Allen MG. Fluid micropumps based on rotary magnetic actuators. Proceedings of MEMS. 1995; **95**:408-412

[10] Mensing G, Pearce T, Bebe DJ. An in-plane active magnetic mixer for microfluidic applications. In: IEEEEMB Conference. 2002. pp. 531-534

[11] Mahmud S, Tasnim SH, Mamun MAH. Thermodynamic analysis of mixed convection in a channel with transverse hydromagnetic effect. International Journal of Thermal Sciences. 2003;**42**:731-740

[12] Miklavcic M. The flow due to a rough rotating disk. Zeitschrift für Angewandte Mathematik und Physik. 2004;**55**:235-246

[13] Mizzi S, Emerson DR, Stefanov SK, Barber RW, Reese JM. Effects of rarefaction on cavity flow in the slip regime. Journal of Computational and Theoretical Nanoscience. 2007;**4**: 817-822

[14] Sparrow EM, Beavers GS, Hung LY. Flow about a porous surface rotating disk. International Journal of Heat and Mass Transfer. 1971;**14**:993-996

[15] Frusteri F, Osalusi E. On MHD and slip flow over a rotating porous disk with variable properties. International Communications in Heat and Mass Transfer. 2007;**14**:34, 492-501

[16] Sparrow EM, Minkowycz WJ, Eckert ERG. Transpiration induced buoyancy and thermal diffusion-diffusion thermo in helium-air free convection boundary layer. ASME Journal of Heat Transfer. 1964;**86**: 508-520

[17] Abdul Maleque K. Magnetohydrodynamic convective heat and mass transfer flow due to a rotating disk with thermal diffusion effect. Journal of Heat Transfer. 2009;**131**:1-8

[18] Afify Ahmed A. Effects of thermal diffusion and diffusion thermo on free convective heat and mass transfer over a stretching surface considering suction or injection. Communications in Nonlinear Science and Numerical Simulation. 2009;**14**:2202-2214

[19] Beg A, Bakier AY, Prasad VR. Numerical study of free convection magnetohydrodynamic heat and mass transfer from a stretching surface to a saturated porous medium with Soret and Dufour effects. Computational Materials Science. 2009;**46**:57-65

[20] Gad-el-Hak M. The fluid mechanics of microdevices. The freeman scholar lecture. Journal of Fluids Engineering-Transactions of the ASME. 1999;**121**: 5-33

[21] Rashed GMA. Chemical entropy generation and MHD effects on the unsteady heat and fluid flow through a porous medium. Journal of Applied Mathematics. 2016;**2016:**9 pages, Article ID 1748312

[22] Cobble MH. Magnetohydrodynamic flow with a pressure gradient and fluid injection. Journal of Engineering Mathematics. 1977;**11**:249-256

[23] Osalusi E, Sibanda P. On variable laminar convective flow properties due to a porous rotating disk in a magnetic field. Romanian Journal of Physics. 2006;**51**(9–10):933-944

[24] Maleque AK, Sattar AM. Steady laminar convective flow with variable properties due to a porous rotating disk. Journal of Heat Transfer. 2005;**127**: 1406-1409